Supporting Information

Chemisorption-Induced Formation of Biphenylene Dimer on Ag(111)

Zhiwen Zeng[1,‡] , Dezhou Guo[2,‡], Tao Wang[1,3,4,*], Qifan Chen[5], Adam Matěj[5], Jianmin Huang[1], Dong Han[1], Qian Xu[1], Aidi Zhao[6], Pavel Jelínek[5], Dimas G. de Oteyza[3,4,7], Jean-Sabin McEwen[2,8,9,10,11,*], Junfa Zhu[1,*]

[1]National Synchrotron Radiation Laboratory, Department of Chemical Physics and Key Laboratory of Surface and Interface Chemistry and Energy Catalysis of Anhui Higher Education Institutes, University of Science and Technology of China, Hefei, 230029, P. R. China.

[2]The Gene & Linda Voiland School of Chemical Engineering and Bioengineering, Washington State University, Pullman, WA 99164, United States.

[3]Donostia International Physics Center, San Sebastián 20018, Spain.

[4]Centro de Fisica de Materiales, CFM/MPC, CSIC-UPV/EHU, San Sebastián 20018, Spain.

[5]Institute of Physics of the Czech Academy of Sciences, Cukrovarnická 10, 16200 Prague 6, Czech.

[6]School of Physical Science and Technology, ShanghaiTech University, Shanghai 201210, China.

[7]Ikerbasque, Basque Foundation for Science, 48013 Bilbao, Spain.

[8]Institute for Integrated Catalysis, Pacific Northwest National Laboratory, Richland, WA 99352, United States.

[9]Department of Physics and Astronomy, Washington State University, Pullman, WA 99164, United States.

[10]Department of Chemistry, Washington State University, Pullman, WA 99164, United States.

[11]Department of Biological Systems Engineering, Washington State University, Pullman, WA 99164, United States.

(1). EXPERIMENTAL METHODS

The experiments were performed in two UHV systems with background pressures better than 2×10^{-10} mbar. The STM and STS measurements were obtained at 4.3 K using low-temperature STM (Omicron GmbH), except a few specially noted STM images where were taken at 85 K using Arhus SPECES STM. CO was deposited onto the sample *via* a leak valve at a pressure of approximately 5×10^{-9} mbar and a maximum sample temperature of 7.0 K. CO was picked up with a metallic W tip when scanning over it using high current (1 nA; -500 mV). Since there are many Br adatoms on the surface, Br was easy to pick up by conventional scanning or tip shaping. The Ag(111) single crystals were cleaned by repeated cycles of bombardment with Ar+ ions and post-annealing to 700 K. The precursor TBBP and DBBP were vapor-deposited from a commercial Kentax evaporator with quartz crucibles held at 330 K and 300 K, respectively. The time for each annealing process at high temperatures was kept in about 30 min. The XPS measurements were performed on the Catalysis and Surface Science Endstation located in National Synchrotron Radiation Laboratory (NSRL), Hefei, China.[1] The XPS spectra were collected at an emission angle of 45° with respect to the surface normal.

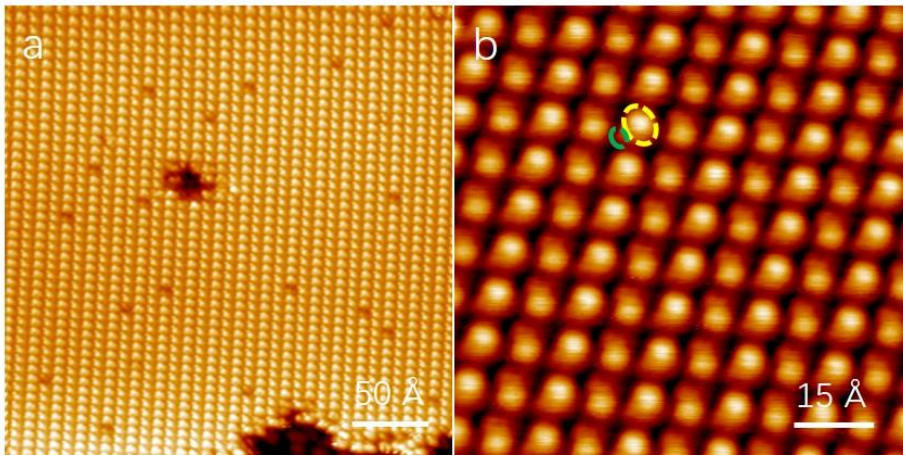

Figure S1. (a, b) overview and magnified STM images obtained after the deposition of TBBP onto Ag(111) surface at a low temperature. Since the manipulator could not be cooled down by liquid nitrogen, the low temperature substrate was obtained by quickly taking the Ag(111) crystal out from the LT-STM held at 78 K, and immediately depositing the molecules. We deduce that the temperature of Ag(111) should be around 250 K. Tunneling parameters: (a, b) U = 1 V, I = 100 pA.

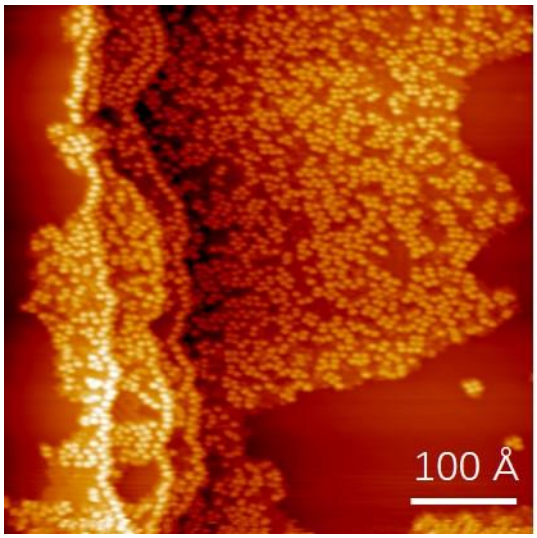

Figure S2. Overview STM image obtained after deposition of TBBP onto Ag(111) held at 300 K. Tunneling parameters: U = 0.5 V, I = 50 pA.

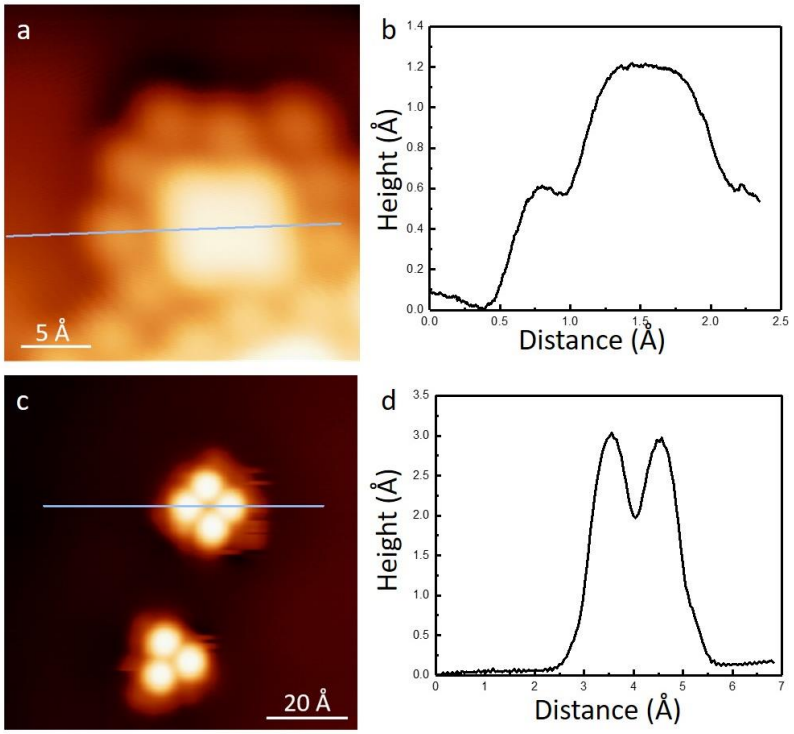

Figure S3. The comparison of the molecular heights on Ag(111) between (a, b) flat biphenylene dimer and (c, d) "stand-up" bi-radical biphenylene. The height curves in (b) and (d) reveal the height changes along the blue lines in STM images (a) and (c), starting from the left side and ending at the right side. The height difference is around 1.8 Å between the two molecules. Tunneling parameters: (a) U = 0.1 V, I = 1 nA; (c) U = 0.1 V, I = 1 nA.

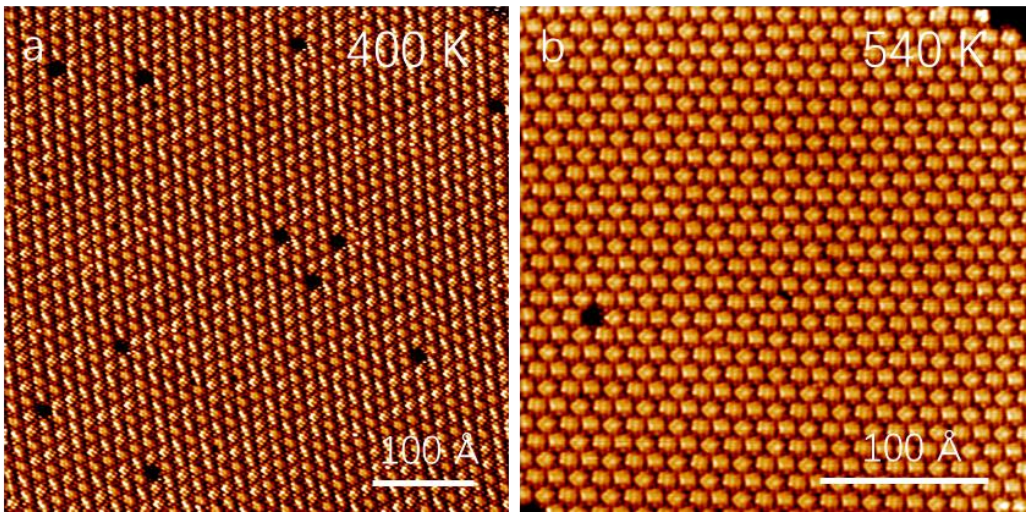

Figure S4. Overview STM image obtained after annealing the RT sample to (a) 400 K and (b) 540 K respectively, using Br functionalized tips. Tunneling parameters: (a,b) U = 0.1 V, I = 1 nA.

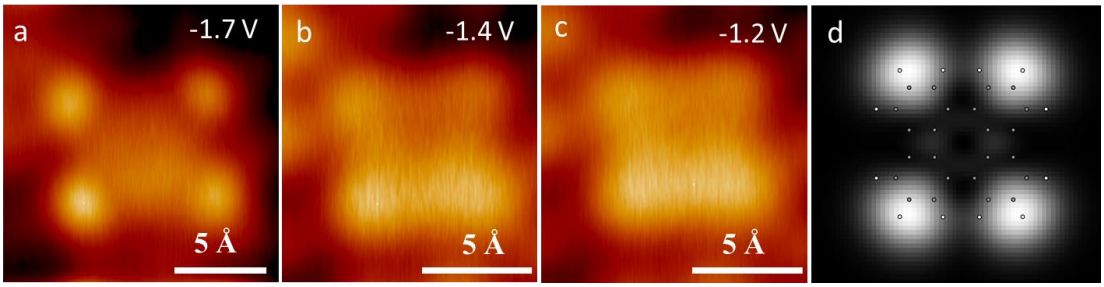

Figure S5. (a-c) Constant-height dI/dV maps of a biphenylene dimer at different negative bias voltages. (d) Simulated dI/dV map corresponding to the HOMO of biphenylene dimer.

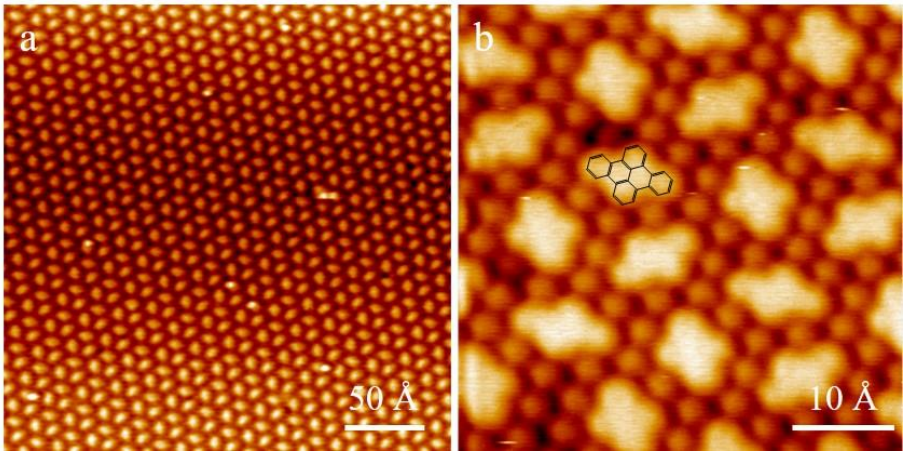

Figure S6. (a, b) Overview and magnified STM images of the sample prepared by deposition of DBBP on Ag(111) held at 450 K. The images were taken at 85 K. Tunneling parameters: (a, b) U = -2 V, I = -0.2 nA.

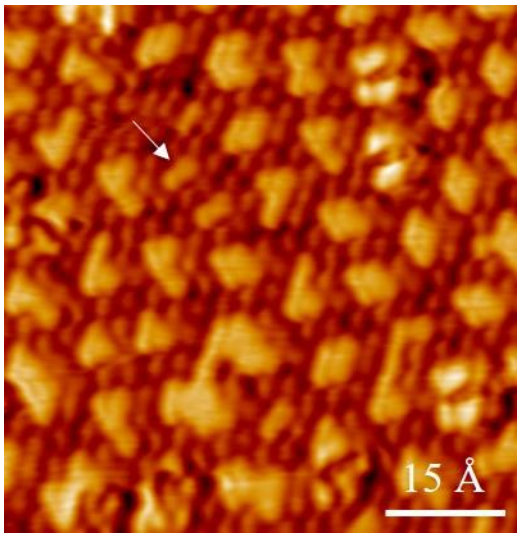

Figure S7. STM image of an area where some byproducts are observed on the sample prepared by deposition of DBBP on Ag(111) held at 550 K. The image was taken at 85 K. The monomers such as the white arrowed pointed one should be biphenylene from intramolecular cycloaddition reaction of DBBP. Note that the major product on this sample is still dibenzo[e,l]pyrene, whose yield is higher than 90%. Some large well-ordered islands of dibenzo[e,l]pyrene were seen on this sample, similar as that in Figure S6a. Tunneling parameters: U = -2 V, I = -0.2 nA.

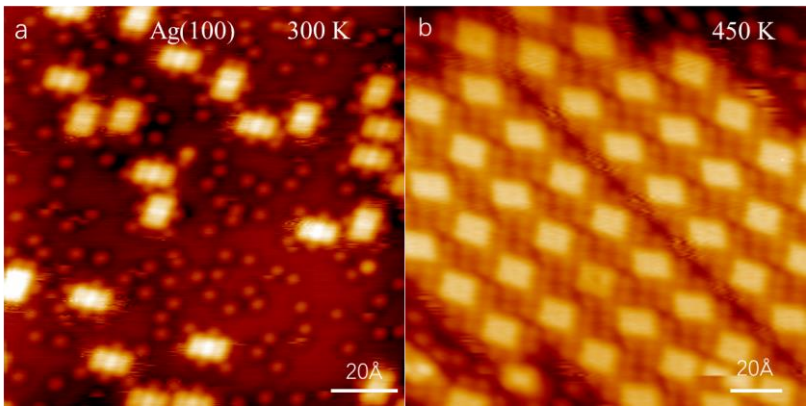

Figure S8. Overview STM images obtained after depositing TBBP molecules on Ag(100) held at (a) 300 K and further annealing to (b) 450 K, respectively. Tunneling parameters: (a) U=-0.5 V, I=0.5 nA; (b) U=-0.1 V, I=1.5 nA;

(2). COMPUTATIONAL DETAILS

A. dI/dV simulations in gas phase

Frontiers molecular orbitals were obtained from density functional theory (DFT) calculations using the FHI-AIMS code[2] within hybrid exchange-correlation functional B3LYP[3-4] for the gas phase molecule. The calculated frontiers HOMO/LUMO orbitals

employed for dI/dV simulations were identical with those obtained with optB86b-vdW functional. Theoretical dI/dV maps were calculated by the Probe Particle Scanning Probe Microscopy (PP-STM) code[9] for a CO-like tip, which was represented by a linear combination of P_xP_y (85%) and s-like (15%) orbitals without tip relaxation.

B. ACID and NICS

Anisotropy of the Induced Current Density (ACID)[5] and nucleus-independent chemical shift (NICS)[6] was calculated in Gaussian16 package[7] at UB3LYP/def2-SVP[8] level of theory and plotted using the code AICD version 3.0.3. Only π-orbitals were included in the calculation.

C. Calculations of TBBP/Ag(111)

DFT simulations using the Vienna *Ab initio* simulation package (VASP) software[10-11] were conducted to simulate the formation processes of 2,2'-dibromo-biphenyl (DBBP) and 2,2',6,6'-tetrabromo-1,1'-biphenyl (TBBP) on Ag(111) surface. Electron smearing was performed with the Gaussian method with a smearing width of 0.2 eV, and the total energy was extrapolated to 0 K. Geometric optimizations were considered converged when the total energy changed by less than 10^{-6} eV and interatomic forces were less than 0.02 eV/Å for the ground state optimizations. The core electrons were described using the projector augmented wave (PAW) method,[12-13] using the PAW potentials that were released in 2015.[14] The valence electrons were modeled using a plane-wave basis set that was expanded to a cutoff energy of 500 eV. The exchange-correlation potential was modeled with the optB86b-vdW functional.[15] Spin-polarization effects were not taken into account in the calculations since the Ag(111) slab is non-magnetic. The structure visualizations were performed with VESTA.[16]

We optimized the bulk Ag lattice using a Monkhorst-Pack (12 × 12 × 12) *k*-point mesh.[17] The optimized cell parameters are $a = b = c = 4.09$ Å from the DFT simulations, which agree very well with the X-ray experimental values of $a = b = c = 4.08$ Å.[18] Thus, the DFT approach describes the crystal structure very well. Then, we cleaved (111) surface and constructed a $p(8\times8)$ Ag (111) slab with four layers. The unit cell of the slab consists of 256 Ag atoms and has a surface area of 23.11 × 20.02 Å[10]. In all geometry optimization calculations, the bottom two layers were fixed at their optimized bulk positions while the top two layers were allowed to fully relax. A vacuum layer of 10 Å and a dipole correction along the *z*-direction were incorporated for eliminating interactions between periodic images of the system.[19] A Monkhorst-Pack (2 × 2 × 1) *k*-point mesh was used.

The harmonic oscillator model of aromaticity (HOMA) was derived from DFT-calculated bond lengths, which takes for benzenoide hydrocarbons Kekulé benzene as a reference, assuming that no π-delocalization effects are encountered other than those in an acyclic polyene. Benzene as the reference molecule has a HOMA value of 1.0. The relationship between the C-C bond length and the HOMA value is described as:

$$\mathrm{HOMA} = 1 - \frac{\alpha}{NB}\sum\left(R_{opt} - R_i\right)^2 \qquad \text{Eq (S1)}$$

In this work, R_{opt} and α take values of 1.393 and 282.94 $Å^{-2}$. NB is the number of C-C bonds in the targeted π-system. R_i denotes an individual C-C bond length in the molecule under consideration.[20]

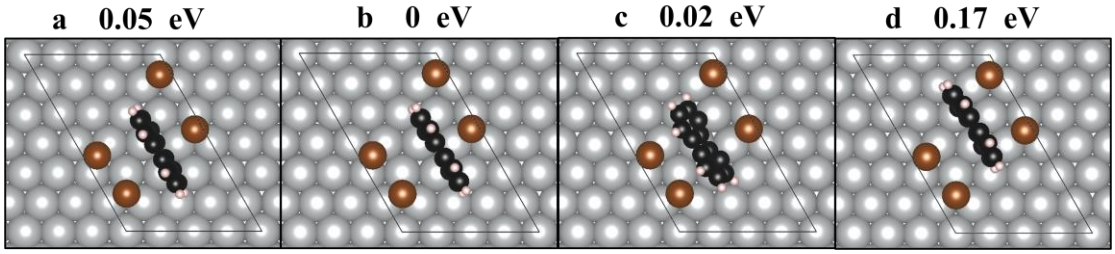

Figure S9. Top views of the possible adsorption configurations of a debrominated TBBP adsorbate on Ag(111). The C, H, Br and Ag atoms are represented by black, pink, brown, and grey spheres, respectively. The perpendicular adsorption configuration (case b) turns out to be the most energetically favorable case, which is shown in Figure 1. Color code: C, black; Ag, grey; H, pink; Br, brown.

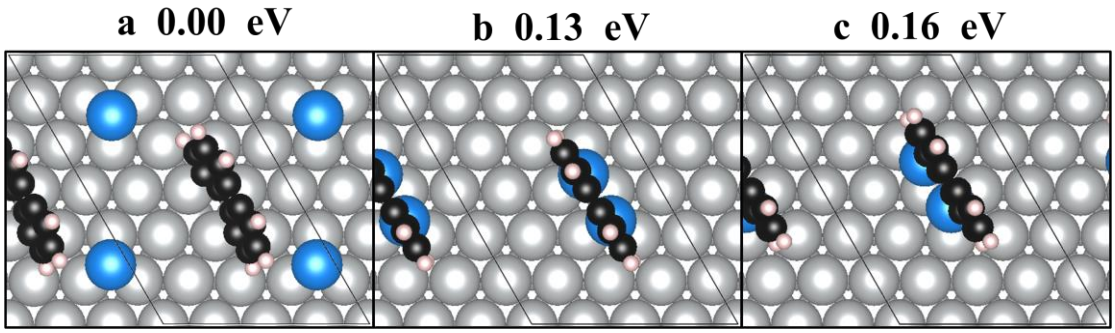

Figure S10. Top views of the adsorption configuration of biphenylene (a) binds with surface Ag atoms (b) binds with add Ag atoms at fcc hollow sites (c) binds with add Ag atoms at hcp hollow sites on Ag(111) surface. The C, H and Ag atoms are represented by black, pink, brown, and grey spheres, respectively. The free Ag adatoms are showed by blue spheres for clarify.

We located the biphenylene adsorbed with these two Ag adatoms at nearby fcc (case b) and hcp (case c) hollow sites, respectively. We found the case that biphenylene binding with surface Ag atoms are energetically favorable.

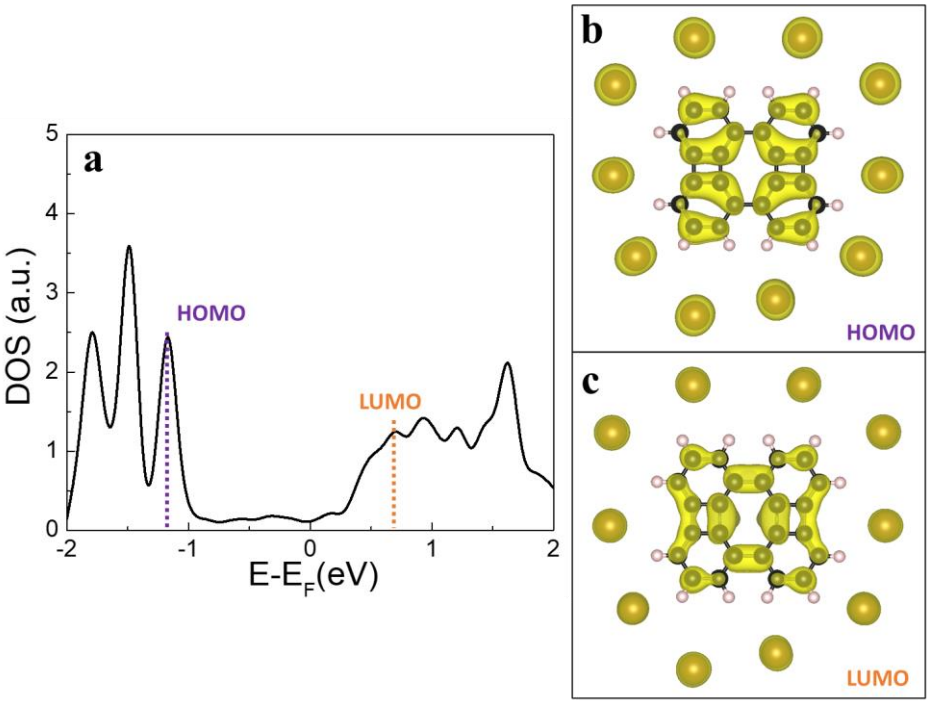

Figure S11. (a) DFT density of states (DOS) analysis of biphenylene dimer adsorbed on the Ag (111) surface. Fermi energy (E_F) is taken to be zero. The corresponding energies of HOMO and LUMO orbitals are marked with a dashed line. (b, c) DFT calculated charge density related to the HOMO and LUMO orbitals of biphenylene dimer on Ag(111) at an isosurface level of 0.001 electrons/Bohr^3 The C, H and Br atoms are represented by black, pink and brown spheres, respectively.

We calculated the DOS based on the computational technique developed by Dronskowski et al.,[21-22] in which the PW/PAW wavefunctions are transferred into a local basis using analytically derived expressions. The PW and PAW eigenstates are reconstructed to a set of Slater-type local orbitals, allowing us to obtain accurate local information from plane wave calculations. The use of this projection scheme resulted in an error of less than 2% for the states of interest and a realistic chemical-bonding picture. Herein, the VESTA[16] program was used to show the configurations and intuitive chemical interpretation.

In order to have a comparable environment of biphenylene dimer in the simulation as in the experiment, the molecule was surrounded by ten Br atoms in our model on Ag (111) surface. The calculated charge density plots related to the HOMO and LUMO orbitals of biphenylene dimer are also shown in Figure S11, which is very similar to those in gas phase as shown in Figure 3f-g, implying a weak interaction between biphenylene dimer and the Ag(111) surface.

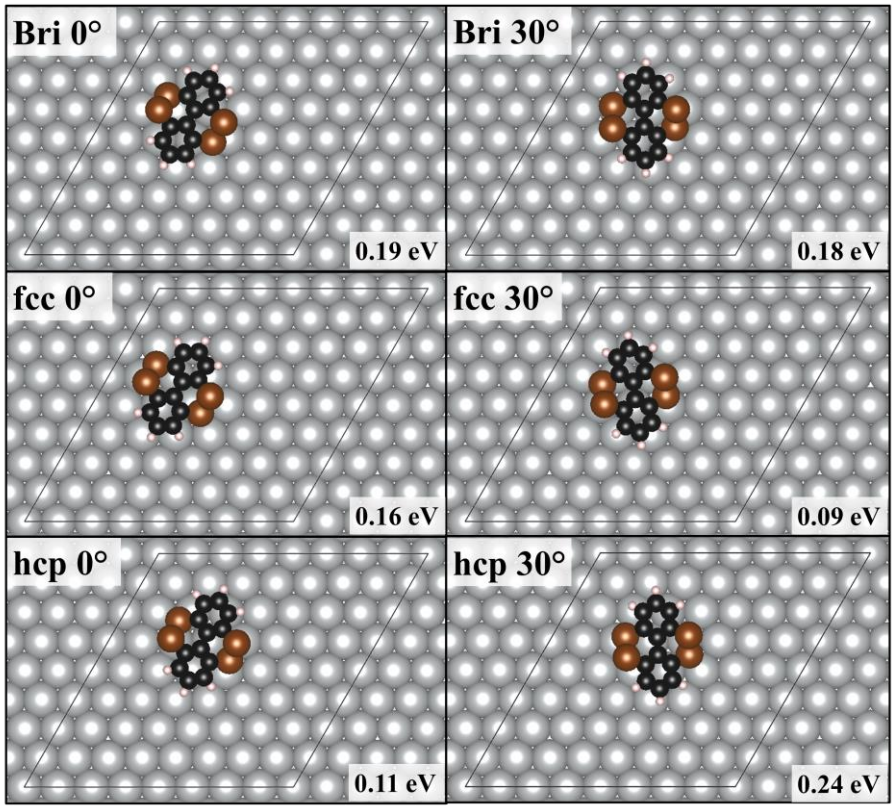

Figure S12. Top view of the optimized structures of TBBP adsorbing at possible adsorption sites on Ag(111). The C, H, Br and Ag atoms are represented by black, pink, brown, and grey spheres, respectively.

Firstly, we systematically checked various adsorption sites on Ag (111) surface using one TBBP molecule to understand its most favorable adsorption configuration. The adsorption energy of the TBBP was calculated as:

$$E_{\text{ads}} = E_{\text{surface+molecule}} - E_{\text{molecule}} - E_{\text{surface}} \qquad \text{(S2)}$$

where $E_{\text{surface+molecule}}$ is the total energy of the system when TBBP adsorbed on Ag (111), E_{surface} is the total energy of the clean Ag surface and E_{molecule} is the isolated energy of TBBP in gas phase.

The possible adsorption sites for adsorption of TBBP on Ag (111) are shown in Figure S12. The adsorption sites are classified by the positions of the center of one out of the two benzene rings in TBBP and the azimuthal angle of TBBP backbone on Ag(111). Bri, fcc and hcp relate to the center of the benzene ring of TBBP at a bridge, fcc hollow and hcp hollow site, respectively. An azimuthal angle of 0° means that the C-C bond of benzene ring is parallel to the $[1\bar{1}0]$ direction of the Ag(111) surface, and a value of 30° means that the C-C bond of the benzene ring is rotated by 30° with respect to the $[1\bar{1}0]$ direction.

The adsorption energy values calculated based on Eq (S2) based on the six distinct sites are plotted in Figure S13. In all cases, the adsorption energy is slightly positive,

revealing that this process is slightly endothermic. The fcc30° site is the most favorable adsorption site for TBBP molecule on Ag (111) with an adsorption energy of 0.09 eV.

We considered this favorable configuration as a starting point of the following TBBP on-surface reactions as shown in Figure 4a in the main text.

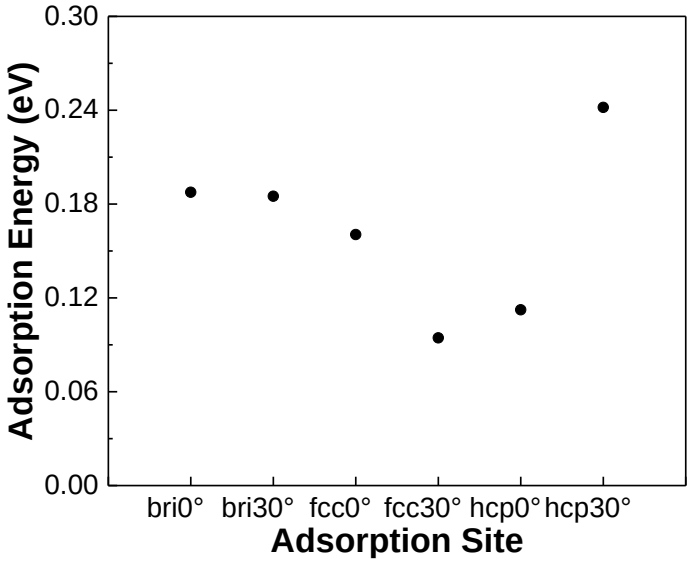

Figure S13. Adsorption energies of TBBP molecule at different adsorption sites as shown in Figure S12.

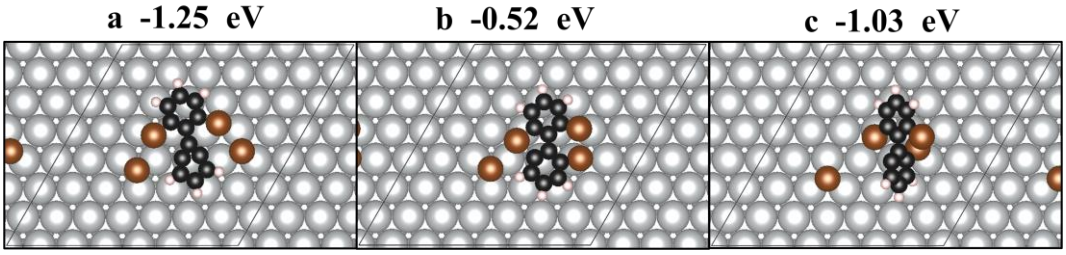

Figure S14. Top view of the optimized possible configurations of TBBP with the first Br atom dissociated on Ag (111). The C, H, Br and Ag atoms are represented by black, pink, brown, and grey spheres, respectively. The total energy of a fcc30° TBBP monomer adsorbate is taken as a reference for the comparison between different adsorbates.

We started these tests with the most favorable adsorption site of TBBP molecule (fcc30° site in Figure S12 in SI) on Ag (111) surface. The Ag (111) surface were modeled by a p(7×7) surface unit cell with three layered slabs separated by 10 Å of vacuum to ensure well-separated molecules between repeated images. After optimization, we found three possible adsorption configurations as shown in Figure S14. Since the configuration of Figure S14a is the most possible configuration with a relative energy of -1.25 eV, we consider it is the final product of the initial debromination process. In fact, it is double confirmed when we tested the transition state of Figure S15.

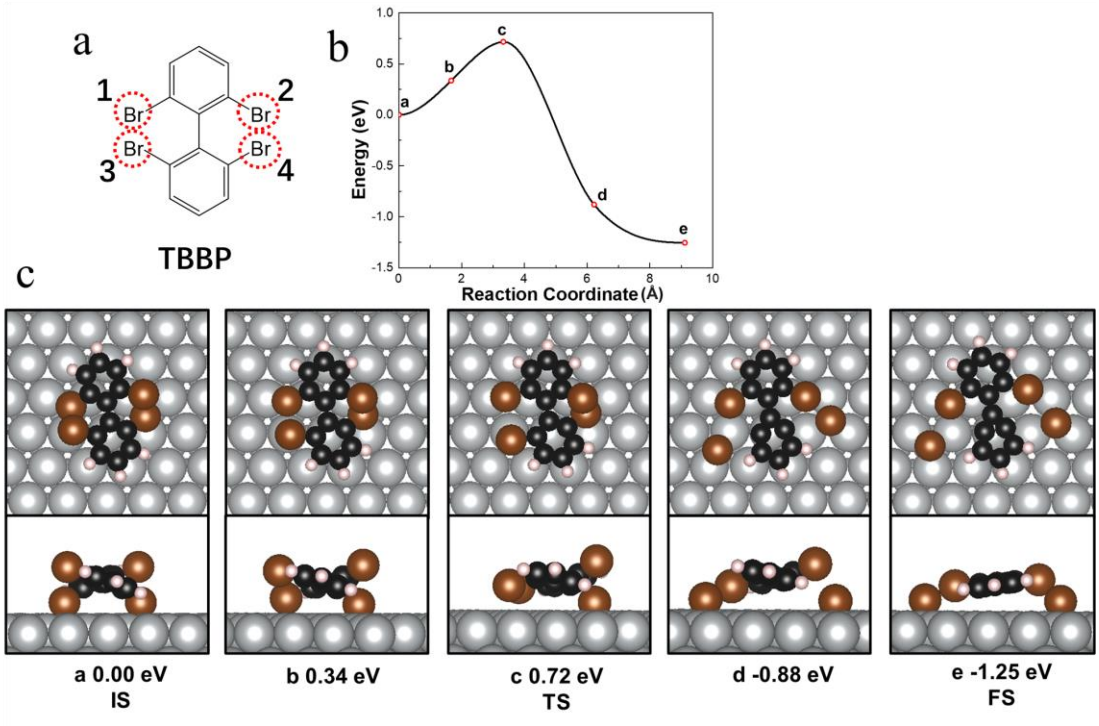

Figure S15. (a) Molecular structure model of TBBP. The four bromine atoms are marked by dashed red circles (sites: 1-4). (b) Energy diagram of debromination reaction. (c) Top and side views of the initial debromination reaction of TBBP on Ag (111). The initial state, transition state and final state are denoted as IS, TS and FS, respectively. The C, H, Br and Ag atoms are represented by black, pink, brown, and grey spheres, respectively. The total energy of initial state is taken as a reference.

The transition-state calculations were carried out with the climbing image nudge elastic band (CINEB) method by finding the saddle points and minimum energy paths between the inert TBBP and the final configuration.[23-24] A number of intermediate images were optimized along the reaction pathway, with the constraints implemented by adding spring forces along the band between images and projecting out the component of the force because of the potential perpendicular to the band. The number of images was adjusted specifically for transition-state calculation such that the tangent along the path was well described. Typically, three to four images were used in these calculations. The structural optimization of the dimer was performed until the forces acting on the atoms on the images were smaller than 0.03 eV/Å.

For IS, TBBP molecule chemisorption with two Br atoms pointing towards the silver surface. Since the two benzene rings are not in the same plane with a dihedral angel of 41.56°, the other two bromine atoms point away from the surface. For FS, however, with the dissociation of two Br atoms at one benzene ring, a deformed ring is observed because two free carbon radicals coordinate with surface silver atoms, indicating the important role of the substrate silver surface in stabilizing the benzene. At this moment, two benzene rings are stay in a same plane. The TS is associated with rotated benzene rings with a smaller dihedral angel of 24.74° compared with that of the IS. The distance

of C-Br bonds is stretched to 2.1 Å (1.9 Å initially). Therefore, Two Br atoms at the same benzene ring (either 1, 2 or 3, 4 sites) will dissociate simultaneously with the energy of 0.72 eV. This excludes the possibility that the intramolecular annulation may also occur as long as two bromines at the same side (either 1, 3 or 2, 4 sites) of molecular backbone dissociated (instead of full debromination).

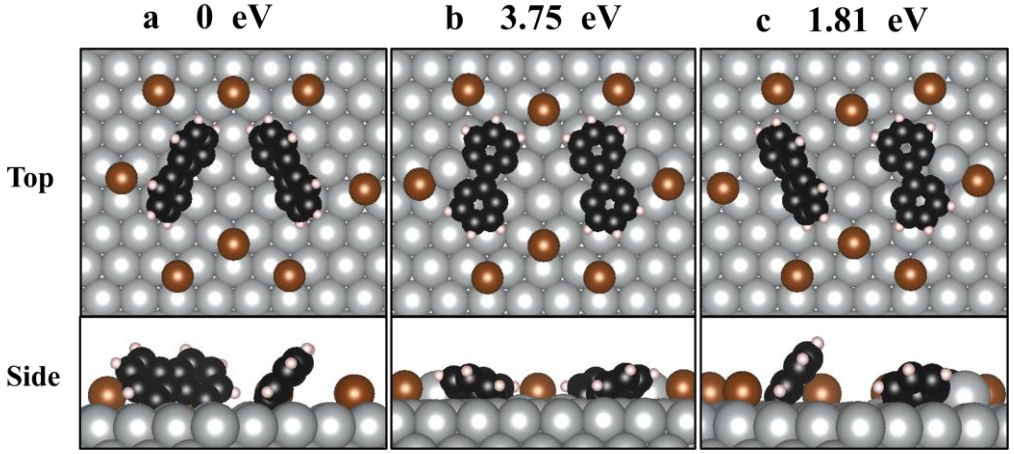

Figure S16. Top and side views of the possible adsorption configurations of debrominated TBBP adsorbing on Ag(111). The C, H, Br and Ag atoms are represented by black, pink, brown, and grey spheres, respectively. Color code: C, black; Ag, grey; H, pink; Br, brown. The total energy of a TBBP monomer (two phenyls and four bromines) on surfaces is taken as the reference for the comparison of energies between different cases, as listed in each picture.

Next, we consider the two-monomer system. To determine the underlying potential energy surface per TBBP monomer adsorbate (Figure 4 in the main text) and per DBBP monomer adsorbate (Figure S19) in these two-monomer systems, we calculated the total adsorption energies of monomers on surfaces in all the reaction steps based on:

$$E_{\text{monomer}} = \frac{1}{2}(E_{\text{system1}} - E_{\text{surface}} - 2 \times E_{\text{molecule}}) \qquad \text{(S3)}$$

where E_{system1} is the total energy of the adsorbate system, E_{surface} is the total energy of the clean Ag (111) surface, and E_{molecule} is the isolated energy of a TBBP or a DBBP molecule in the gas phase.

After the full debromination of the TBBP, we found two possible pathways, *i.e.* the four-radical biphenyl either undergoes intramolecular annulation reaction to form bi-radical biphenylene monomer, or bonds with surface Ag adatom to form Ag-biphenyl complex. Hence, there are three possible configurations: case a involves two bi-radical biphenylene monomer, case b is two Ag-biphenyl complex and case c shows one bi-radical biphenylene monomer and one Ag-biphenyl complex. Case a is the most energetically favorable configuration, which is shown in Figure 4a. Both the adjacent biphenylene monomers are slightly tilted instead of being perpendicular to the surface

due to their intermolecular interaction, as seen in Figure S16a. They will coordinate with two Ag adatoms to form an organometallic dimer in the next step, as shown in Figure 4a.

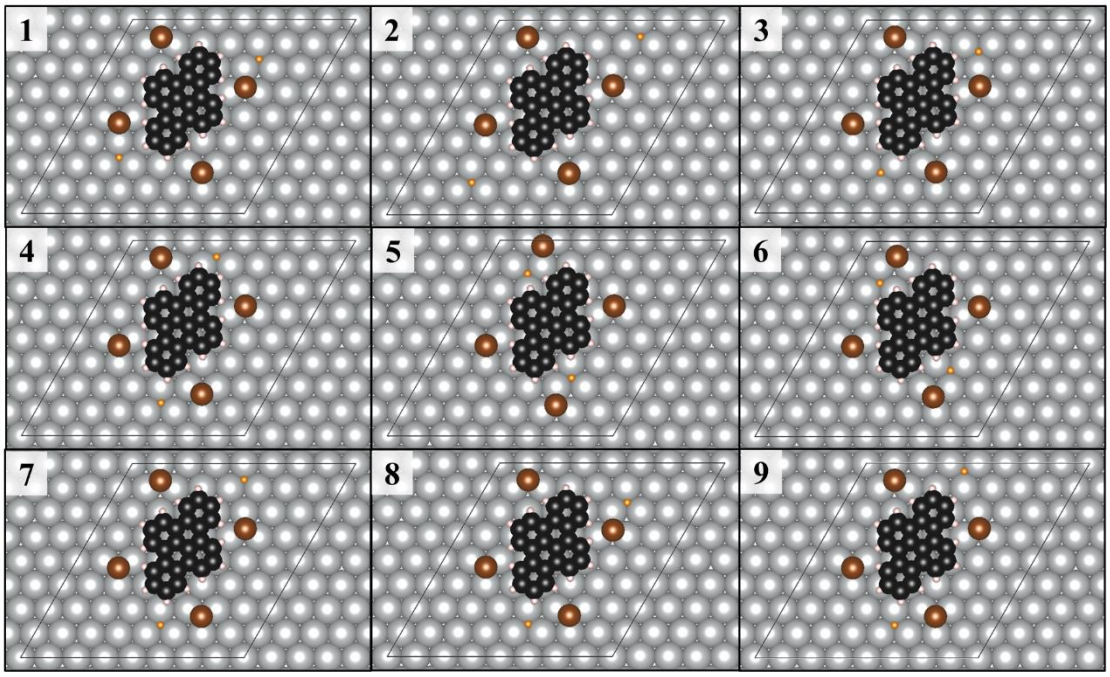

Figure S17. Possible configurations of dibenzo[e,l]pyrene nanographene adsorbing on Ag(111). The different positions of dissociated H atoms on Ag (111) surface have different energies as shown in Figure S18. The C, H, Br and Ag atoms are represented by black, pink, brown, and grey spheres, respectively. The dissociated H atoms are represented by orange spheres for clarity.

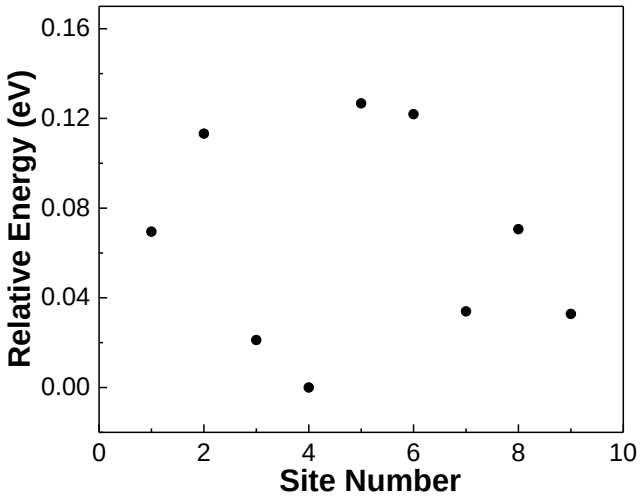

Figure S18. Relative energies for the possible configurations of dibenzo[e,l]pyrene nanographene adsorbing on Ag(111) surface as shown in Figure S17. Case 4 is the most favorable configuration.

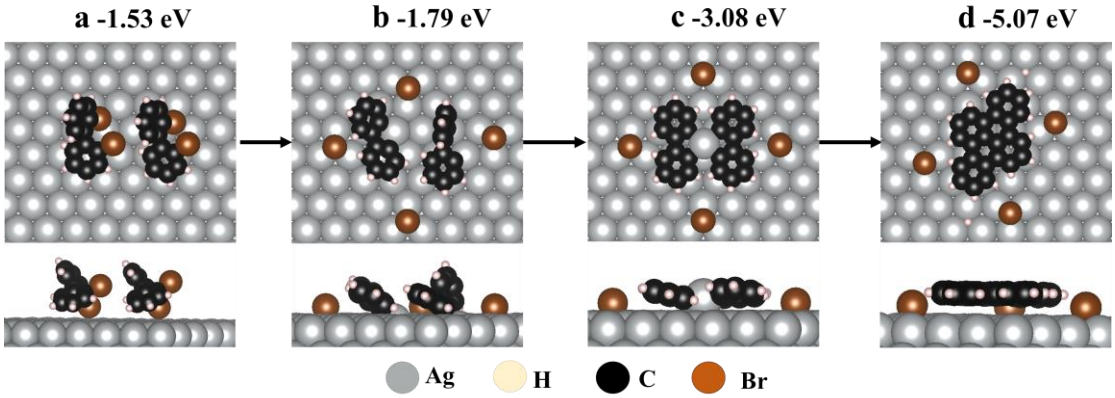

Figure S19. Optimized geometries of the reaction evolution of DBBP to dibenzo[e,l]pyrene nanographene on Ag(111). The C, H, Br and Ag atoms are represented by black, pink, brown, and grey spheres, respectively. The total adsorption energies (calculated with the Eq S3) of the DBBP monomer in each structure on the Ag(111) surface are given.

The reaction of DBBP is an exothermic reaction where the energy diagram goes downhill in each reaction step. Firstly, unlike the endothermic adsorption of TBBP, the intact DBBP adsorbs strongly on the surface with the adsorption energy of -1.53 eV. Then, the dissociation of Br atoms is much less exothermic for DBBP as compared to TBBP (-0.26 *vs.* -3.97 eV). A Ag-biphenyl complex is produced with two radicals stabilized by one underneath surface silver atom. Next, an organometallic dimer with four-fold C-Ag bonds are formed, which planarize the structure and further lower the energy of the system. Finally, dibenzo[e,l]pyrene is formed through Ullmann coupling followed by the cyclodehydrogenation, after the release of the interstitial Ag adatom in the organometallic dimer.

REFERENCES

(1) Ju, H.; Knesting, K. M.; Zhang, W.; Pan, X.; Wang, C. H.; Yang, Y. W.; Ginger, D. S.; Zhu, J. Interplay between Interfacial Structures and Device Performance in Organic Solar Cells: A Case Study with the Low Work Function Metal, Calcium. *ACS Appl. Mater. Interfaces* **2016,** *8*, 2125-2131.

(2) Blum, V.; Gehrke, R.; Hanke, F.; Havu, P.; Havu, V.; Ren, X.; Reuter, K.; Scheffler, M. Ab initio Molecular Simulations with Numeric Atom-Centered Orbitals. *Comput. Phys. Commun.* **2009,** *180*, 2175-2196.

(3) Becke, A. D. A New Mixing of Hartree-Fock and Local Density-Functional Theories. *J. Chem. Phys.* **1993,** *98*, 1372-1377.

(4) Lee, C.; Yang, W.; Parr, R. G. Development of the Colle-Salvetti Correlation-Energy Formula into A Functional of The Electron Density. *Phys. Rev. B: Condens. Matter Mater. Phys.* **1988,** *37*, 785-789.

(5) Herges, R.; Geuenich, D. Delocalization of Electrons in Molecules. *J. Phys. Chem. A* **2001,** *105*, 3214-3220.

(6) Schleyer, P. V. R.; Maerker, C.; Dransfeld, A.; Jiao, H.; van Eikema Hommes, N. J. R. Nucleus-Independent

Chemical Shifts: A Simple and Efficient Aromaticity Probe. *J. Am. Chem. Soc.* **1996,** *118*, 6317-6318.

(7) M. J. Frisch, G. W. T., H. B. Schlegel, G. E. Scuseria, M. A. Robb, J. R. Cheeseman, G. Scalmani, V. Barone, G. A. Petersson, H. Nakatsuji, X. Li, M. Caricato, A. V. Marenich, J. Bloino, B. G. Janesko, R. Gomperts, B. Mennucci, H. P. Hratchian, J. V. Ortiz, A. F. Izmaylov, J. L. Sonnenberg, D. Williams-Young, F. Ding, F. Lipparini, F. Egidi, J. Goings, B. Peng, A. Petrone, T. Henderson, D. Ranasinghe, V. G. Zakrzewski, J. Gao, N. Rega, G. Zheng, W. Liang, M. Hada, M. Ehara, K. Toyota, R. Fukuda, J. Hasegawa, M. Ishida, T. Nakajima, Y. Honda, O. Kitao, H. Nakai, T. Vreven, K. Throssell, J. A. Montgomery, Jr., J. E. Peralta, F. Ogliaro, M. J. Bearpark, J. J. Heyd, E. N. Brothers, K. N. Kudin, V. N. Staroverov, T. A. Keith, R. Kobayashi, J. Normand, K. Raghavachari, A. P. Rendell, J. C. Burant, S. S. Iyengar, J. Tomasi, M. Cossi, J. M. Millam, M. Klene, C. Adamo, R. Cammi, J. W. Ochterski, R. L. Martin, K. Morokuma, O. Farkas, J. B. Foresman, and D. J. Fox Gaussian 16, Revision C.01. Gaussian, Inc., Wallingford CT. **2016**.

(8) Weigend, F.; Ahlrichs, R. Balanced Basis Sets of Split Valence, Triple Zeta Valence and Quadruple Zeta Valence Quality for H to Rn: Design and Assessment of Accuracy. *Phys. Chem. Chem. Phys.* **2005,** *7*, 3297-3305.

(9) Krejčí, O.; Hapala, P.; Ondráček, M.; Jelínek, P. Principles and Simulations of High-Resolution STM Imaging with A Flexible Tip Apex. *Phys. Rev. B* **2017,** *95*, 045407.

(10) Kresse, G.; Furthmuller, J. Efficient Iterative Schemes for Ab Initio Total-Energy Calculations Using a Plane-Wave basis set. *Phys. Rev. B: Condens. Matter Mater. Phys.* **1996,** *54*, 11169-11186.

(11) Kresse, G.; Hafner, J. Ab Initio Molecular Dynamics for Liquid Metals. *Phys. Rev. B: Condens. Matter Mater. Phys.* **1993,** *47*, 558-561.

(12) Kresse, G.; Joubert, D. From Ultrasoft Pseudopotentials to the Projector Augmented-Wave Method. *Phys. Rev. B: Condens. Matter Mater. Phys.* **1999,** *59*, 1758-1775.

(13) Blochl, P. E. Projector Augmented-wave Method. *Phys. Rev. B: Condens. Matter Mater. Phys.* **1994,** *50*, 17953-17979.

(14) Lejaeghere, K.; Bihlmayer, G.; Bjorkman, T.; Blaha, P.; Blugel, S.; Blum, V.; Caliste, D.; Castelli, I. E.; Clark, S. J.; Dal Corso, A.; de Gironcoli, S.; Deutsch, T.; Dewhurst, J. K.; Di Marco, I.; Draxl, C.; Dulak, M.; Eriksson, O.; Flores-Livas, J. A.; Garrity, K. F.; Genovese, L.; Giannozzi, P.; Giantomassi, M.; Goedecker, S.; Gonze, X.; Granas, O.; Gross, E. K.; Gulans, A.; Gygi, F.; Hamann, D. R.; Hasnip, P. J.; Holzwarth, N. A.; Iusan, D.; Jochym, D. B.; Jollet, F.; Jones, D.; Kresse, G.; Koepernik, K.; Kucukbenli, E.; Kvashnin, Y. O.; Locht, I. L.; Lubeck, S.; Marsman, M.; Marzari, N.; Nitzsche, U.; Nordstrom, L.; Ozaki, T.; Paulatto, L.; Pickard, C. J.; Poelmans, W.; Probert, M. I.; Refson, K.; Richter, M.; Rignanese, G. M.; Saha, S.; Scheffler, M.; Schlipf, M.; Schwarz, K.; Sharma, S.; Tavazza, F.; Thunstrom, P.; Tkatchenko, A.; Torrent, M.; Vanderbilt, D.; van Setten, M. J.; Van Speybroeck, V.; Wills, J. M.; Yates, J. R.; Zhang, G. X.; Cottenier, S. Reproducibility in density functional theory calculations of solids. *Science* **2016,** *351*, aad3000.

(15) Klimeš, J.; Bowler, D. R.; Michaelides, A. Chemical Accuracy for the Van der Waals Density Functional. *J. Phys.: Condens. Matter* **2009,** *22*, 022201.

(16) Momma, K.; Izumi, F. VESTA 3 for Three-Dimensional Visualization of Crystal, Volumetric and Morphology Data. *J. Appl. Crystallogr.* **2011,** *44*, 1272-1276.

(17) Platt, P.; Frankel, P.; Gass, M.; Howells, R.; Preuss, M. Finite Element Analysis of the Tetragonal to Monoclinic Phase Transformation during Oxidation of Zirconium Alloys. *J Nucl Mater* **2014,** *454*, 290-297.

(18) Davey, W. P. Precision Measurements of the Lattice Constants of Twelve Common Metals. *Phys Rev* **1925,** *25*, 753-761.

(19) Neugebauer, J.; Scheffler, M. Adsorbate-Substrate and Adsorbate-Adsorbate Interactions of Na and K Adlayers on Al(111). *Phys. Rev. B: Condens. Matter Mater. Phys.* **1992,** *46*, 16067-16080.

(20) Setiawan, D.; Kraka, E.; Cremer, D. Quantitative Assessment of Aromaticity and Antiaromaticity Utilizing

Vibrational Spectroscopy. *J. Org. Chem.* **2016,** *81*, 9669-9686.
(21) Maintz, S.; Deringer, V. L.; Tchougreeff, A. L.; Dronskowski, R. Analytic Projection from Plane-Wave and PAW Wavefunctions and Application to Chemical-Bonding Analysis in Solids. *J. Comput. Chem.* **2013,** *34*, 2557-2567.
(22) Deringer, V. L.; Tchougreeff, A. L.; Dronskowski, R. Crystal Orbital Hamilton Population (COHP) Analysis as Projected from Plane-Wave Basis Sets. *J. Phys. Chem. A* **2011,** *115*, 5461-5466.
(23) Henkelman, G.; Jonsson, H. Improved Tangent Estimate in the Nudged Elastic Band Method for Finding Minimum Energy Paths and Saddle Points. *J. Chem. Phys.* **2000,** *113*, 9978-9985.
(24) Henkelman, G.; Uberuaga, B. P.; Jonsson, H. A. A Climbing Image Nudged Elastic Band Method for Finding Saddle Points and Minimum Energy Paths. *J. Chem. Phys.* **2000,** *113*, 9901-9904.